SEMARAK ILMU PUBLISHING

CFD Letters

Journal homepage:
https://semarakilmu.com.my/journals/index.php/CFD_Letters/index
ISSN: 2180-1363

Computational Study of Pump Turbine Performance Operating at Off-Design Condition-Part I: Vortex Rope Dynamic Effects

Muhannad Altimemy[1,*], Ahmed Khalid Ibrhim[2], Hassan Raheem Hassan[1], Mustaf Jabbar Hayawi[3]

[1] Department of Materials Engineering, College of Engineering, Al-Shatrah University, Thi-Qar, Iraq
[2] Department of Mechanical Engineering, College of Engineering, University of Mosul, Mosul, Iraq
[3] Department of Computer Engineering, College of Engineering, Al-Shatrah University, Thi-Qar, Iraq

ARTICLE INFO

Article history:
Received 10 February 2024
Received in revised form 11 March 2024
Accepted 10 April 2024
Available online 31 October 2024

Keywords:
Numerical study; large-eddy simulations; pressure oscillation; partial load; pump-turbine: vortex rope; unsteady flow

ABSTRACT

As global power demand increases, hydropower plants often must operate beyond their optimal efficiency to meet grid requirements, leading to unstable, high-swirling flows under various load conditions that can significantly shorten the lifespan of turbine components. This paper presents an in-depth computational study on the performance and dynamics of a pump-turbine operating under 80% partial load, focusing on the formation and impact of vortex ropes. Large Eddy Simulation (LES) was utilized to model the turbulent flow, revealing complex patterns and significant pressure fluctuations. A pronounced straight vortex rope was identified in the draft tube, maintaining its trajectory and core size consistently, profoundly affecting flow characteristics. Pressure fluctuations were observed at various cross-sectional planes, with peaks and troughs primarily near the runner, indicating areas prone to instability. The standard deviation of pressure fluctuations ranged from 4.51 to 5.26 along the draft tube wall and 4.27 to 4.97 along the axial center, highlighting significant unsteady flow. Moreover, the frequency corresponding to the highest amplitude in pressure coefficient spectrographs remained consistent at approximately 9.93 to 9.95, emphasizing the persistent influence of vortex rope dynamics. These dynamics affected power generation, which was approximately 29.1 kW, with fluctuations accounting for about 3% of the total generated power, underscoring the critical impact of vortex rope formation on the performance and operational stability of pump-turbines under off-design conditions. This study provides essential insights vital for enhancing the design and operational strategies of these turbines, ensuring more efficient and reliable energy production in the face of increasing power demands.

1. Introduction

The present power advancement is oriented towards an extensive penetration of renewable power resources in the electrical grid. Using the new energy sources will undoubtedly boost the stochastic part of the electrical power manufacturing, which might lead to unwanted voltage variations and harmonic distortion in the network, potentially threatening the stability of the electrical supply. To guarantee a secure electricity supply, the equilibrium between power generation

* *Corresponding author.*
muhannadsahib@shu.edu.iq (Muhannad Altimemy)

https://doi.org/10.37934/cfdl.17.3.148166

and usage needs to be ensured all the time. Since hydro turbines produce electricity rapidly, reliably, and with high quality, Francis, Kaplan, and Pump turbine units have the demand to enhance the operation regime flexibility, during load acceptance and rejections [1–5], to achieve a fast response time to the changing in the electric power consumptions. However, due to the inherent structural characteristics of the Francis turbine, unsteady swirling flows occur at the off-design conditions which limit the operating range of the turbine. Unfortunately, partial load operating conditions cause the incident of undesirable flow phenomena such as draft tube vortices, vortex shedding, and cavitation, which create large pressure oscillations and reveal the units to the threats of structural damage [6–11]. Thus, it is required to check and evaluate the state of turbines and take targeted measures to enhance the stability of the unit.

At partial load operating conditions, the flow field in hydro turbines becomes unstable in the draft tube causing the vortex rope formation [12–14]. Various flow instabilities like stagnant point, recirculation region, and flow separation are assumed as the origins of rotating vortex rope creation [15–17]. This leads to reductions in the overall efficiency of the turbine unit. Furthermore, the complex interaction between the guide vanes and the runner introduces an output torque oscillation as well as asymmetric and unsteady forces on the surfaces of the blades [18–21]. A strong vortex rope precession easily visualizes inside the draft tube under off-design operating regimes [22–25]. The vortex rope has a very unsteady nature, and its form can be significantly altered over time [26,27]. Skripkin *et al.,*[28] studied the dynamics of the vortex rope and its trajectory in one revolution of precession for different flow rate amounts. The amplitudes of the pressure pulsations were highly dependent on the trajectory as well as the strength of the vortex rope [29]. The helical motion of the vortex rope is associated with a high amplitude, low-frequency pressure fluctuations [30–34].

The characteristics of the vortex rope and the physics behind its formation were investigated during the load variation [35]. Four various flow regimes with different features were recognized. First, at the optimal load condition, the flow regime is a stable swirling structure. The initial indicators of flow instabilities show up immediately at the beginning of the transition from the best efficiency point to partial load operating condition. With high load rejection, the flow becomes more instabilities and creates the vortical structures in the draft tube. The fourth flow regime is the presence of an established rotating vortex rope occurring at a certain point according to the size and shape of the unit. The effect of load variation on the pressure fluctuations applied on a Kaplan turbine runner was also investigated [36–38]. The vortex rope precession produces pressure pulsations in the axial and rotating directions known as plunging and rotating modes, respectively. The plunging mode induced flow oscillation throughout the entire turbine conduit, while the rotating mode resulted in local pressure fluctuations. The formation of the vortex rope is due to significant pressure differences on the suction side of the blade, resulting in pronounced penstock vibrations and noticeable fluctuations in output power [39–42].

A numerical study was carried out to deeply investigate the vortex rope movement and associated pressure pulsation during its development inside a Francis turbine [43]. In general, two modes of revolutions with the same rotating direction can be recognized. The first is a revolution around the axis of the draft tube center, and the second mode is a revolution around the core of the vortex rope. The elliptical-shaped vortex rope causes synchronous and asynchronous pressure fluctuations inside the draft tube [44]. To our knowledge, prior research has not used high-fidelity Large Eddy Simulations (LES) to explore the impact of vortex ropes on flow-induced pressure fluctuations and the power performance of pump turbines [45]. In this study, a complex three-dimensional turbulent flow throughout the whole flow passage of a pump-turbine operating in a turbine mode is simulated using a high-fidelity Large Eddy Simulation (LES) turbulence model. The

pump-turbine is utilized at off-design load with 80% of the optimal flow rate, 0.16 m^3/s. The computational domain consists of three components: volute, runner blades, and draft tube. Several probes are installed in the unit to observe pressure fluctuation inside the draft tube, which can help to evaluate the unit stability. In the meantime, the frequencies corresponding to the highest amplitude of the pressure fluctuation were identified using Fast Fourier Transformation (FFT). Contours of velocity, vorticity, and iso-surfaces of Q-criterion are acquired within the draft tube and on the runner blades. The overall purpose is to assess pump-turbine performance, efficiency, and output power.

2. Mathematical Model and Numerical Method

Numerical simulations are performed using the finite volume discretization method. The pressure-based segregated solver was used to solve the continuity and momentum equations simultaneously. Simulations are conducted using the Segregated Semi-Implicit Method for Pressure-Linked Equations (SIMPLE) algorithm with the Pressure Staggering Option (PRESTO) scheme adopted for the pressure correction, as recommended for high-speed rotating flows [46]. The second-order discretization schemes were used.

Large Eddy Simulation decomposes the turbulent flow into Grid-Scale (GS) eddies which are larger than the grid size and Sub-Grid Scale (SGS) eddies which are smaller than the grid size. Large-scale eddies ($\langle u\rangle, \langle p\rangle$) were resolved explicitly, while small eddies ($\tilde{u}, \tilde{p}$) were modeled by implementing a subgrid-scale (SGS) model. The spatial filtering is applied to Navier-Stokes's equations [47]:

$$\frac{\partial\langle u_i\rangle}{\partial x_i} = 0 \tag{1}$$

$$\frac{\partial\langle u_i\rangle}{\partial t} + \langle u_j\rangle\frac{\partial\langle u_i\rangle}{\partial x_j} = -\frac{1}{\rho}\frac{\partial\langle p\rangle}{\partial x_i} - \frac{\partial\tau_{ij_{SGS}}}{\partial x_j} + \frac{\partial}{\partial x_j}\left(\nu\frac{\partial\langle u_i\rangle}{\partial x_j}\right) \tag{2}$$

where $\langle u_i\rangle = u_i - \tilde{u}_i$ is the filtered velocity vector. The overbar represents the filtering operator; $\tilde{p}$ is the resolved pressure, ρ is the fluid density. The second term in Eq. (2) is unknown quantities named sub-grid shear stress.

$$\begin{aligned}\tau_{ij_{SGS}} &= \langle u_i u_j\rangle - \langle u_i\rangle\langle u_j\rangle \\ &= \langle(\langle u_i\rangle + \tilde{u}_i)\big(\langle u_j\rangle + \tilde{u}_j\big)\rangle - \langle u_i\rangle\langle u_j\rangle \\ &= \underbrace{\langle\langle u_i\rangle\langle u_j\rangle\rangle - \langle u_i\rangle\langle u_j\rangle}_{①} + \underbrace{\langle\langle u_i\rangle\tilde{u}_j + \langle u_j\rangle\tilde{u}_i\rangle}_{②} + \langle\tilde{u}_i\tilde{u}_j\rangle\end{aligned} \tag{3}$$

On the right side of Eq. (3), both first and second terms have almost the same values and the effects of these two terms are normally neglected because they cancel out each other. The sub-grid shear stress is modeled by the subgrid-scale (SGS) model using the Boussinesq hypothesis. The SGS turbulent stress is calculated in the following equations [47]:

$$\tau_{ij_{SGS}} = \langle\tilde{u}_i\tilde{u}_j\rangle = \frac{1}{3}\delta_{ij}k_{SGS} - \nu_{SGS}\left(\frac{\partial\langle u_i\rangle}{\partial x_j} + \frac{\partial\langle u_j\rangle}{\partial x_i}\right) \tag{4}$$

where δ_{ij} is the Kronecker delta, k_{SGS} is SGS turbulence kinetic energy and ν_{SGS} is the SGS eddy viscosity. Wall-adapting local eddy-viscosity (WALE)-SGS model is used to model the eddy viscosity ν_{SGS}. It is defined in the previous study [48].

$$\nu_{SGS} = L_s^2 \frac{\left(S_{ij}^d S_{ij}^d\right)^{3/2}}{\left(S_{ij}S_{ij}\right)^{5/2} + \left(S_{ij}^d S_{ij}^d\right)^{5/4}} \tag{5}$$

$$S_{ij} = \frac{1}{2}\left(\frac{\partial\langle u_i\rangle}{\partial x_j} + \frac{\partial\langle u_j\rangle}{\partial x_i}\right) \tag{6}$$

$$G_{ij} = \frac{\partial\langle u_i\rangle}{\partial x_j} \tag{7}$$

$$S_{ij}^d = \frac{1}{2}\left(G_{ij}^2 + G_{ji}^2\right) - \frac{\delta_{ij}}{3}\, G_{kk}^2 \tag{8}$$

$$G_{ij}^2 = G_{ik} * G_{kj} \tag{9}$$

$$L_s = min\left(Ky, C_w V^{1/3}\right) \tag{10}$$

Where L_s are the sub-grid scales mixing length, K is the von Karman constant, y is the first cell thickness near the wall, the value of the WALE constant, C_w is 0.325, and the cell volume is V. The eddy-viscosity will be nearly zero in areas close to walls without the application of any damping function. The detailed description of the WALE model is documented by previous study [48].

3. Computational Domain and Meshing

The computational domain is intricately designed, consisting of a runner, a simplified volute, and a straight-shaped draft tube, with the volute and draft tube serving as stationary subdomains and the runner operating as a rotational subdomain. These components are interconnected through non-conformal meshes, which are crucial for the exchange of flow variables at each iteration, thereby enhancing the simulation precision and effectiveness. Detailed representations of the runner are provided through both plane and meridional views in Figure 1, offering a comprehensive visual understanding of its structure, while Table 1 meticulously lists the relevant dimensions and specifications. The design of the runner blade is informed by previously reported data [49]. The effects of turbine blade design on turbine performance are very crucial [50–55].

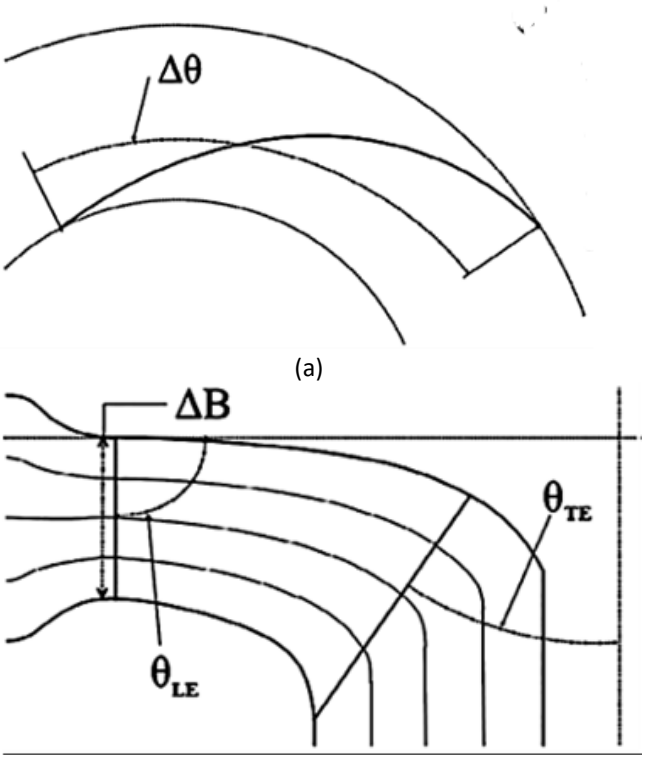

Fig. 1. (a) Plane and (b) meridional view of the runner [49]

Table 1
Runner design variables [49]

Variable	Description	Value
ΔB	Gate height	$67.133\ mm$
$\Delta\theta_{hub}$	Blade wrap angle at the hub	74.729^o
$\Delta\theta_{shroud}$	Blade wrap angle at the shroud	34.304^o
θ_{LE}	Leading-edge lean angle	88.697^o
θ_{TE}	Trailing edge lean angle	37.669^o

The three-dimensional representation of the pump-turbine system is depicted in Figure 2, offering a detailed visualization of its components. The runner, detailed in Figure 2(a), comprises six blades and has a diameter of D = 0.41m, while the total length of the draft tube extends to four times the diameter (4D). To monitor pressure fluctuations, probes are placed along the wall and the center of the draft tube domain, specifically labeled as A1-A9 and C1-C9 as illustrated in Figure 2(b). The system operates at a volumetric flow rate of $0.16\ m^3/s$ corresponding to 80% partial load. At the main water inlet, the flow direction is 6^o to the circumferential direction, with a total head of 31.6 m. A no-slip boundary condition is meticulously applied to the surfaces of both the runner and the draft tube. The outflow boundary condition, ensuring a zero-gradient velocity normal to the surface, is employed at the outlet. The runner rotation speed is precisely set at 1200 rpm. The Reynolds number, calculated to be 1.06×10^7 according to the IEC 60193 Standard [56], follows the formula $Re = \pi n D_{ref}^2/(60\nu)$, where n is the rotation rate, D_{ref} is the reference blade tip diameter at the hub, and ν is the kinematic viscosity of the water (m^2/s).

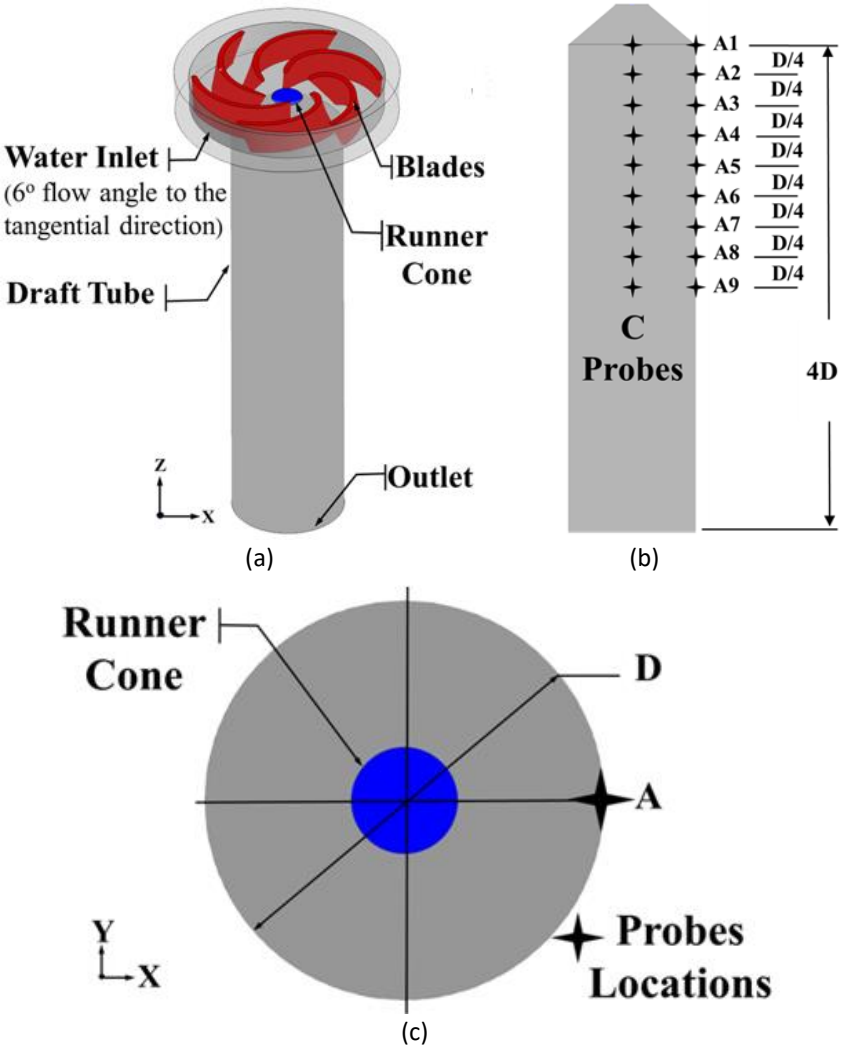

Fig. 2. Comprehensive schematic of the computational domain: (a) three-dimensional view of the pump-turbine unite (b) side view of the draft tube (c) top view of the draft tube. Included are the locations of pressure probes along the wall of the draft tube (A) and at the center (C), as indicated in (b) and (c)

The mesh structure for the runner blades and the draft tube is meticulously illustrated in Figure 3, where the magnified images highlight the use of finer mesh at the edges of the blade and the draft tube walls to accurately resolve near-wall turbulent flow structures. A total mesh density of 62 million elements is employed across the simulation: 30 million mesh elements are dedicated to the runner region, another 30 million to the draft tube, and the remaining 2 million to the volute domain. This extensive meshing ensures a comprehensive and precise capture of fluid dynamics across the system. Additionally, the mean y^+ , which is a crucial parameter for evaluating the adequacy of near-wall mesh in turbulence modelling, is predicted to be approximately 5 along the surface of the runner blade, indicating an effectively optimized mesh for capturing the intricate flow characteristics.

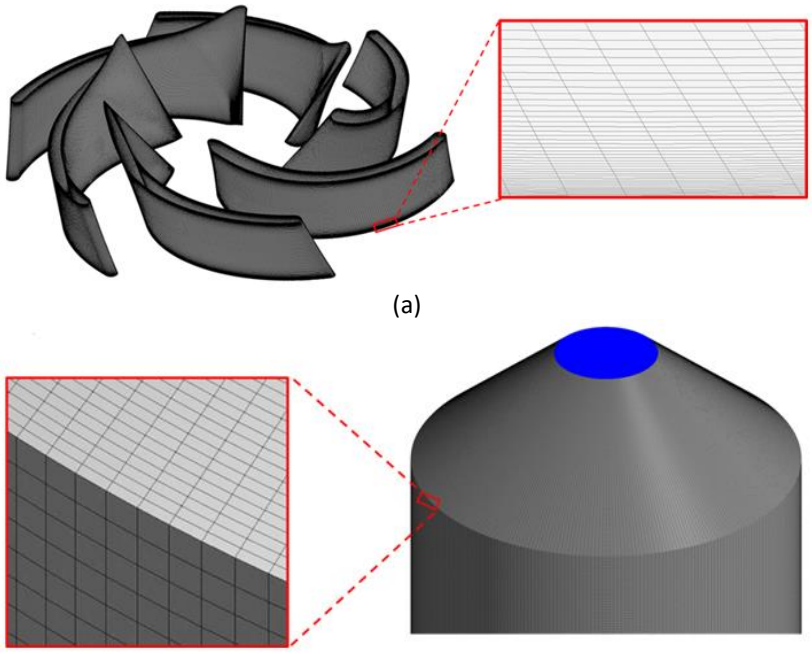

Fig. 3. Detailed mesh configuration, show casing (a) the blade surface and (b) the surfaces of the draft tube. Magnified images show the detailed structure of the mesh near the edges

The power spectrum density (PSD) of the pressure coefficient signal is depicted in Figure 4. The pressure signatures are acquired at the probe locations A1 and C1 within the draft tube domain. The power spectrum demonstrates a decay with a slope of approximately $-5/3$, indicating that the Large Eddy Simulation (LES) model employed is adept at capturing both the temporal and spatial characteristics of eddies and their complex interactions, as substantiated by references [57,58]. This detail underscores the model proficiency in simulating the nuanced dynamics of turbulent flows.

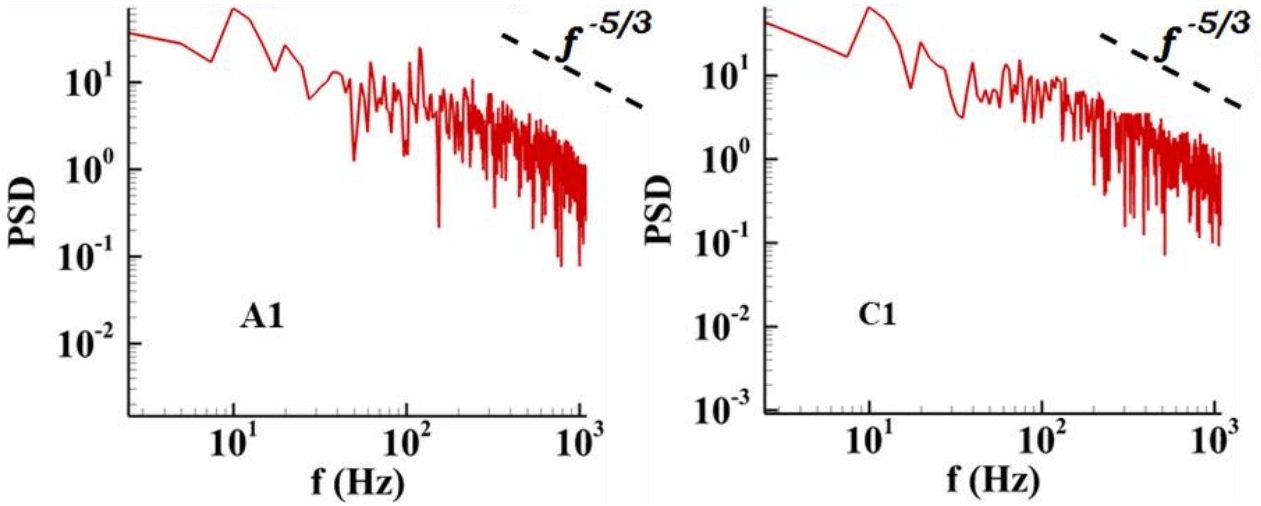

Fig. 4. Power spectral density (PSD) of the pressure coefficient signatures. Pressure signatures were acquired at probes located (a) draft tube wall, and (b) draft tube center using a mesh density of 62 million. The predicted PSD decay slope of −5/3 is indicated

4. Results

Large Eddy Simulation (LES) simulations were conducted under an 80% partial load operating condition, aiming to thoroughly characterize the complex turbulent flow dynamics within a pump-turbine. This included detailed analyses of velocity and pressure fields in both the draft tube and runner regions. Numerous probes were used to investigate flow-induced high-pressure fluctuations throughout the draft tube. Probes were located at the center and on the draft tube wall. The velocity and vorticity field presented are normalized by the reference blade tip diameter at the hub, $\pi n D_{ref} \,/\, 60$ and the rotation rate, $\pi n \,/\, 60$, respectively. The pressure field is presented as the pressure coefficient:

$$C_P = \frac{P - P_{average}}{\rho g H} \tag{11}$$

Where H is the head of the turbine, g is the magnitude of the gravitational acceleration, and $P_{average}$ is the average pressure.

Instantaneous contours of velocity, vorticity, and pressure and the iso-surfaces of Q-criterion in the draft tube with 80% of the design flow rate are illustrated in Figure 5. Rendered at the turbine 14^{th} revolution, the images reveal a prominent, straight vortex rope at the center of the draft tube. This rope, originating from the runner region at the inlet of the draft tube, extends toward the outlet with minimal or no dissipation, as depicted in Figure 5(c). The vortex rope maintains its straight trajectory and uniform core size continuously to the draft tube exit, indicating its sustained strength and stability throughout the draft tube. The constant cross-sectional area of the draft tube significantly contributes in preserving the intensity of the vortex rope. Moreover, the presence of the vortex rope profoundly impacts the spatial and temporal flow characteristics within this region, manifesting as low pressure and high vorticity, particularly along the draft tube center as illustrated in Figure 5(a) and Figure 5(d). The flow images further reveal a gradient in pressure, with low pressure observed along the central axis and progressively increasing in the radial direction.

At the inlet of the draft tube, particularly near the blade region, there is a notable concentration of small-scale eddies. As shown in Figure 5(a) and Figure 5(c), these vortex filaments wrap around the vortex rope downstream and then rapidly dissipate further downstream. By the midpoint of the draft tube, the vorticity filaments almost completely vanish. This high prevalence of both large and small eddies near the draft tube entrance is a direct consequence of the highly turbulent flow conditions originating in the blade region. This turbulence is primarily due to the conversion of the high flow energy into dynamic energy by the rotating pump-turbine shaft, which results in a bulk flow energy loss and the generation of eddies of varying lengths with energy higher than that of the remaining flow. As these small vortices dissipate and turbulence diminishes in the stream-wise direction away from the runner region, the density and intensity of these vortical structures decrease, indicating a transition towards more stable flow conditions and the conversion of dynamic energy into static energy throughout the draft tube. The interplay between the vortex rope, small-scale vortical structures, and their mutual interactions within the draft tube significantly impacts flow-induced high-pressure fluctuations and can induce harmful vibrations. Hydro turbines are susceptible to cavitation instabilities. It is a well-documented phenomenon that cavitation often occurs within the vortex rope inside the draft tube of hydro turbines, especially when operating under partial load conditions, as noted in reference [59].

Elevated levels of vorticity are predicted near the central region of the draft tube, correlating with low-velocity zones, as demonstrated in Figure 5(a) and Figure 5(b). The velocity contours reveal

significant swirling around the turbine walls, contrasting with the slower flow at the center of the draft tube. This suggests a stagnant region in the draft tube center, indicating that the pump-turbine design channels minimal fluid straight behind the runner domain in this area. Instead, most of the fluid is directed near the draft tube wall, attributed to the high swirl velocity associated with the partial load condition, as noted in reference [59]. Both velocity and pressure increase radially away from the draft tube center, clearly demonstrating the significant impact of the vortex rope presence. The shear layer within the draft tube is discernible in the pressure contours, where the pressure dips in the center due to the vortex rope and rises closer to the walls in the radial direction. The interface between the low and high-pressure zones marks the shear layer, resulting from a disparity in vorticities between the central and wall regions, as depicted in Figure 5(a), Figure 5(c), and Figure 5(d). This complex interplay of forces and flows within the draft tube is critical for understanding and optimizing turbine performance.

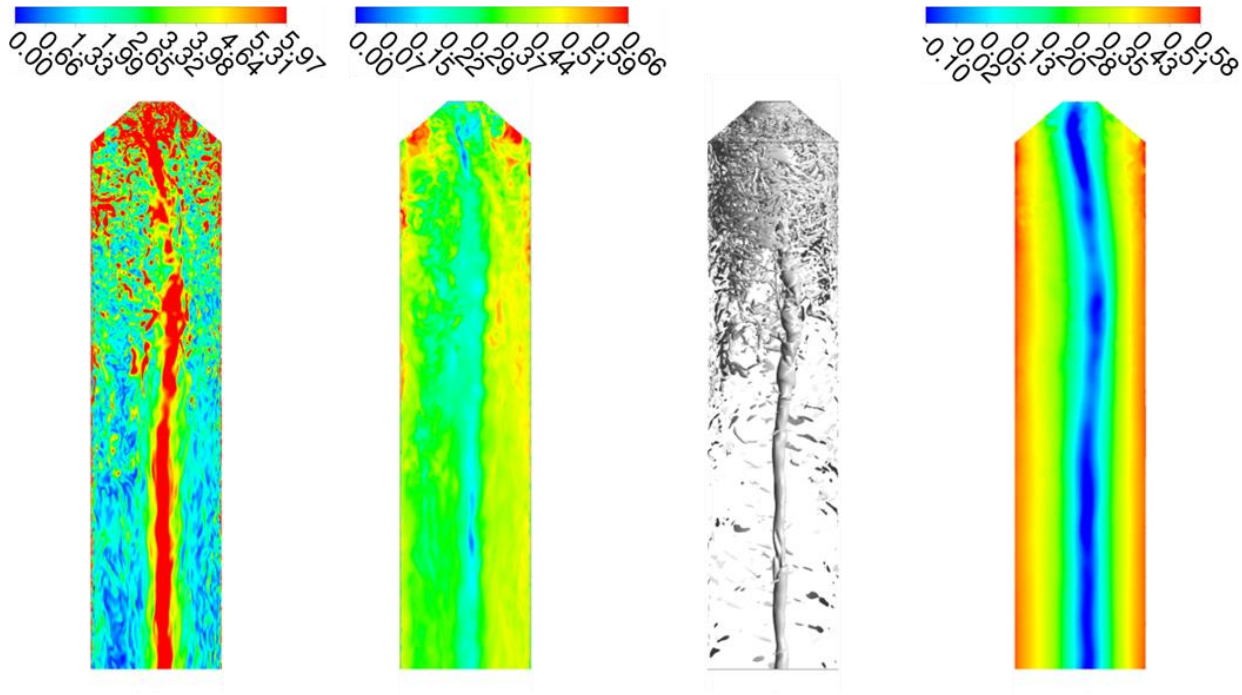

(a) (b) (c) (d)

Fig. 5. The instantaneous contours of (a) dimensionless vorticity, (b) dimensionless velocity, (c) iso-surfaces of Q-criterion, and (d) instantaneous contours of pressure coefficient during the partial load 80% of the design point flowrate. Images are rendered at the center plane of the draft tube at the turbine 14^{th} revolutions

Figure 6 displays instantaneous contours of the pressure coefficient within the draft tube, captured at various cross-sectional planes. These planes correspond to probe locations A1, A3, A6, and A9, denoted as locations (A-D) respectively. The contours reveal that the maximum and minimum pressure values are primarily located at the plane A1, which is closely related to the effects of the runner. This finding indicates that the region nearest to the runner is most prone to pressure fluctuations. As the flow progresses further down the draft tube, the pressure gradually decreases and becomes more uniform, reflecting a significant reduction in the influence of turbulent flow. Additionally, a strong negative pressure coefficient, marked by the blue color in the center of the draft tube, denotes regions at risk of cavitation, typically aligning with the vortex rope location. Downstream, the negative pressure gradually increases toward zero, promoting an improved

pressure distribution along the draft tube cross-sectional planes. This pattern confirms that most high-pressure oscillations in the draft tube are primarily caused by the runner impact and the vortex rope movement. When moving radially away from the vortex rope, there is an increase in pressure, illustrating the intricate pressure dynamics within the pump-turbine system and the significant effects of the vortex rope.

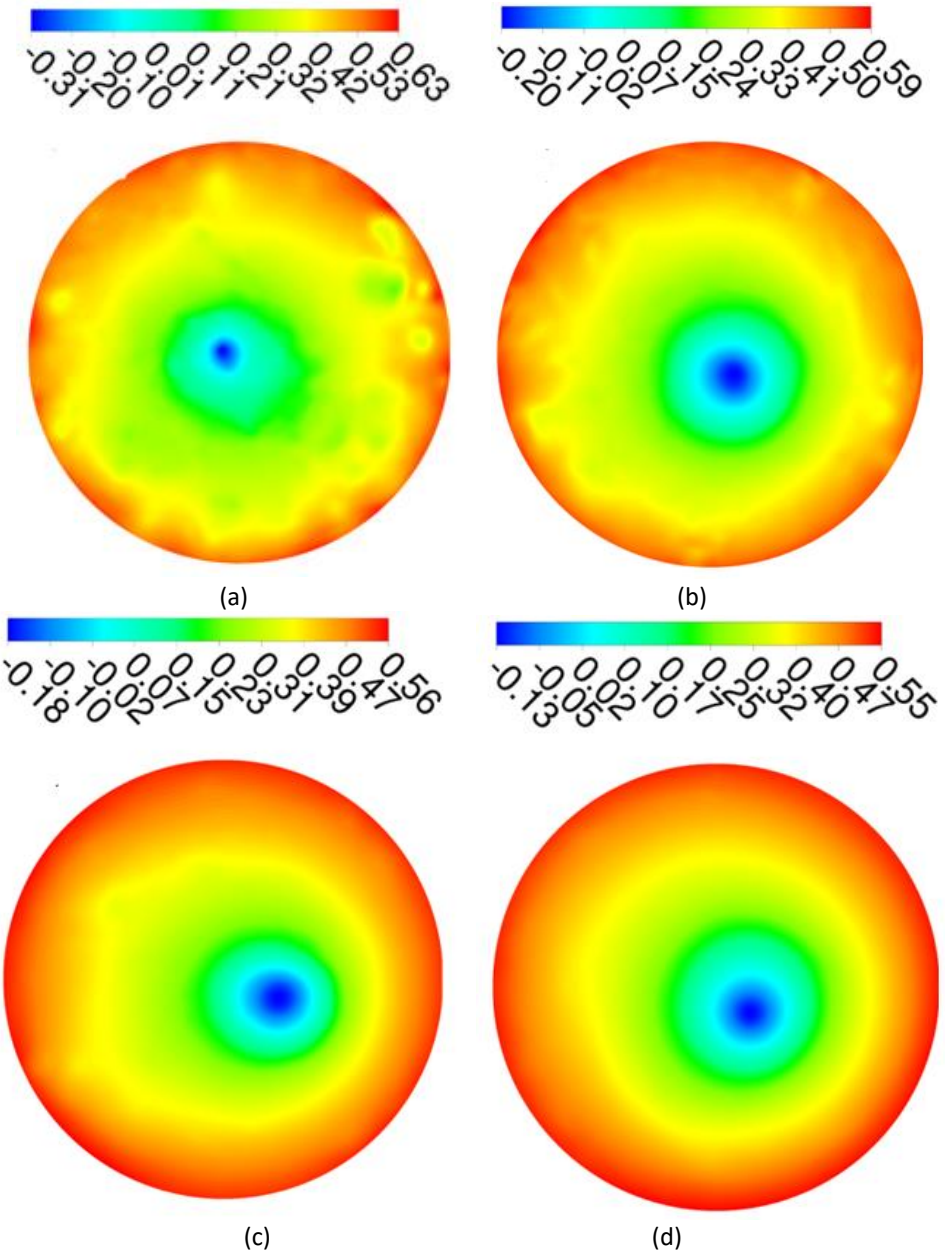

Fig. 6. The instantaneous contours of the pressure coefficient with various cross-section planes of the draft tube (a) at A1 sensor location in the draft tube entrance, (b) at A3 sensor location with 0.5D distance from the draft tube entrance, (c) at A6 sensor location with 1.25D distance from the draft tube entrance, (d) at A9 sensor location with 2D distance from the draft tube entrance

Figure 7 presents normalized velocity contours at the same cross-sectional planes as those for the pressure coefficient. In all plane locations, a low-velocity region is observed in the center of the

draft tube, surrounded by an area of high swirling velocity magnitude at the outer region, where the velocity increases radially. A stagnant region is notably present in the vortex rope area. The high swirl flow structures near the draft tube wall are promoted instabilities for pump-turbine operations. The cross-section plane at the runner exists has a much larger velocity component compared than the others, due to the high energy of the turbulent flow at the draft tube inlet. The magnitude of velocity decreases along the streamwise axis as the vortical activity decreases. As the flow goes further through the draft tube, the dynamic flow energy converts to static energy, and flow becomes slow and more uniform velocity distribution.

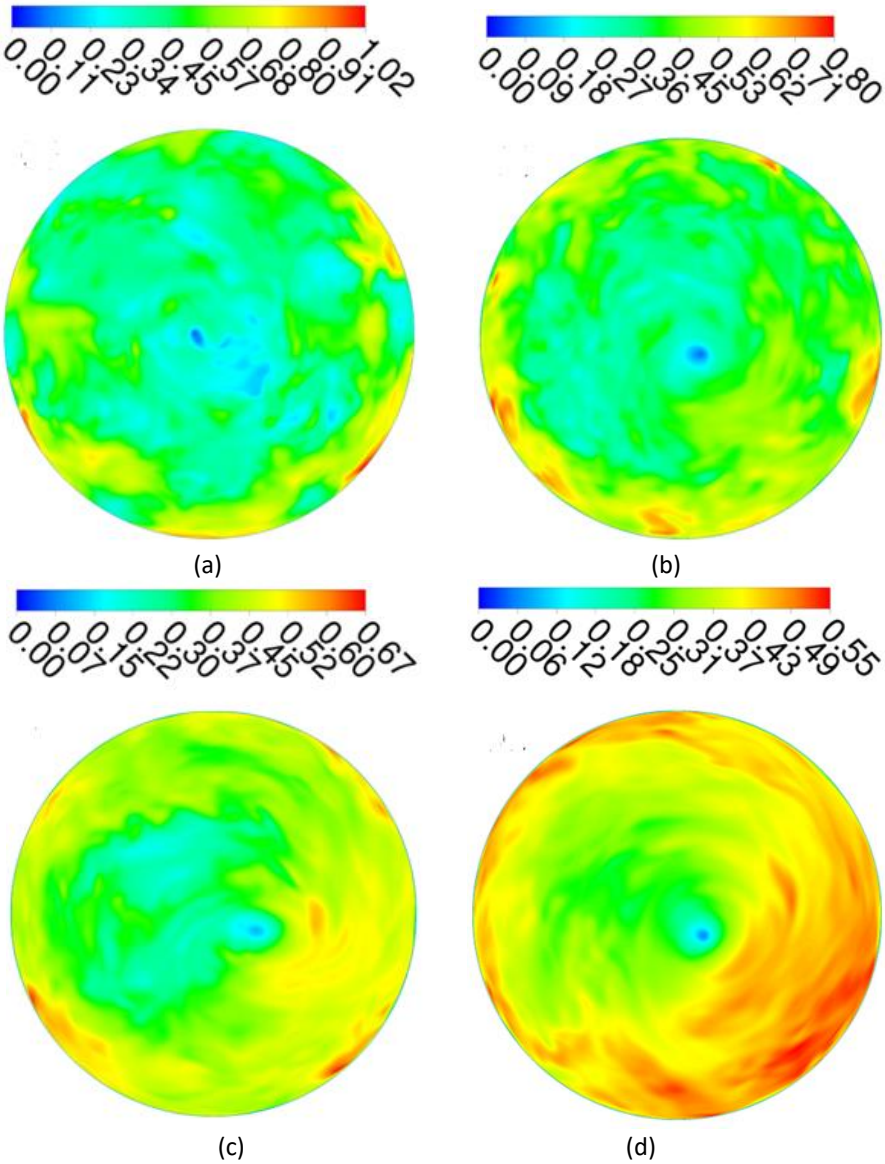

Fig. 7. The instantaneous contours of the velocity with various cross-section planes of the draft tube (a) at A1 sensor location in the draft tube entrance, (b) at A3 sensor location with 0.5D distance from the draft tube entrance, (c) at A6 sensor location with 1.25D distance from the draft tube entrance, and (d) at A9 sensor location with 2D distance from the draft tube entrance

Figure 8 illustrates the pressure contours within the runner region, which are indicative of typical turbine operation patterns. As expected, the pressure is higher in the outer region and decreases

toward the inner region along the blade surfaces. There is a uniform pressure distribution across the blades, registering at a magnitude of 1. The maximum pressure is identified at the blade tip, the primary point of contact for the incoming flow. Additionally, on the pressure side, there is a gradual decrease in the pressure coefficient from the outer region to the inner region, extending towards the trailing edge. Conversely, the minimum pressure occurs on the suction side near the leading edge, resulting from the narrow gap between the volute and the blade, which leads to rapid decreases in pressure. The significant pressure differential between the high and low-pressure sides has the potential to generate a vortex rope and a collection of small-scale vortices in the vicinity of the runner region within the draft tube, highlighting the complex dynamics that influence turbine performance and efficiency.

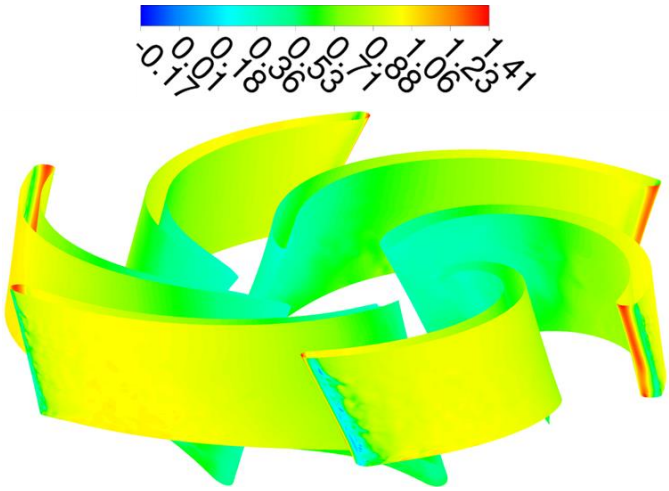

Fig. 8. The instantaneous contours of pressure coefficient along the runner surfaces

Figure 9 shows the pressure signals probed at the draft tube wall A1-A9 and draft tube center C1-C9 as a function of the turbine revolution. The fluctuating component of the pressure coefficient, $\acute{C}_P$, presented in Figure 9 is defined as:

$$\acute{C}_P(x_i, t) = C_P(x_i, t) - \overline{C_P}(x_i) \tag{12}$$

where $\overline{C_P}(x_i) = (1/T) \int C_P(x_i, t)dt$ is the pressure coefficient time-averaged over the period T. Across all locations, the pressure signals exhibit at least two modes: one characterized by high-frequency, low amplitude, and the other by high amplitude with low-pressure fluctuation, particularly in regions affected by the vortex rope. The consistency of pressure signals across all probe locations suggests that the vortex rope maintains its strength throughout the downstream flow in the draft tube. However, such high levels of fluctuations pose a risk to the structural integrity and stable operation of the unit, potentially reducing the service life of the equipment due to exposure to dynamic loading. The standard deviation of the pressure coefficient, as detailed in Table 2, highlights the intensity of these fluctuations, with notable variances near the blade exit at probe A1 due to the high concentration of small eddies at the draft tube entrance. Despite these variances, there is an overall uniform pressure intensity suggesting a persistent, strong vortex rope, indicative of a highly unsteady flow that might affect system stability.

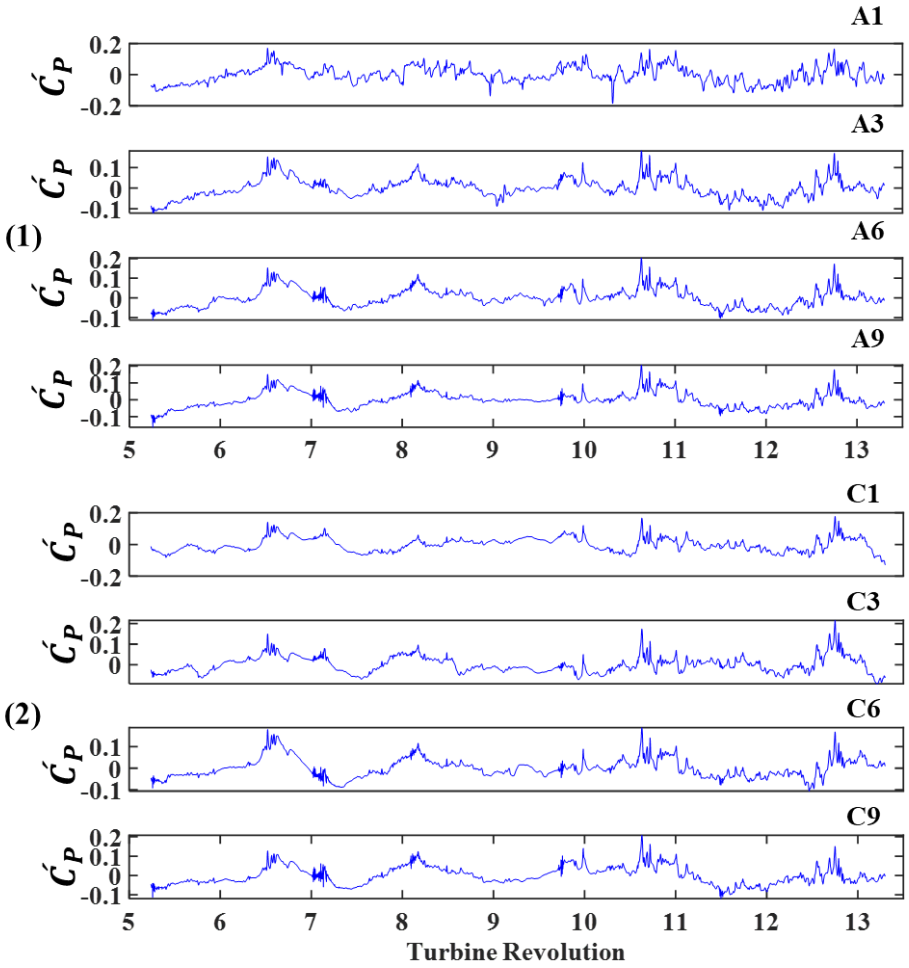

Fig. 9. The pressure coefficients as a function of turbine revolutions during the partial load operation regime. The pressure signals are probed at (1) draft tube wall A1-A9 and (2) draft tube center C1-C9 as indicated in each graph

Table 2
The standard deviation of pressure fluctuation intensity normalized by the total head of the water

Probe locations	Draft tube wall (A)	Draft tube center (C)
1	5.264	4.519
2	4.714	4.974
3	4.679	4.975
4	4.725	4.279
5	4.587	4.639
6	4.552	4.488
7	4.533	4.398
8	4.680	4.619
9	4.640	4.672

In addition to calculating the standard deviation of the pressure coefficient, the Fourier Transform of the pressure signal (FFT) is illustrated in Figure 10. The frequency corresponding to the maximum amplitude fluctuation is identified in Table 3. The power spectrum of the pressure coefficients is depicted, with the right column representing data from the wall of the draft tube and the left column

from the center. Similar to the findings presented in the pressure coefficient Figure 9 and Table 2, alongside the low amplitude, high-frequency modes, there is a consistent spike observed across all probes. High amplitude and low-frequency fluctuations remain the predominant mode throughout the draft tube. Given the presence of small eddy structures near the draft tube wall, the intensity of pressure fluctuations is slightly elevated in that region. These high amplitude fluctuations pose a significant risk of causing major damage and could eventually lead to fatigue in the pump-turbine unit.

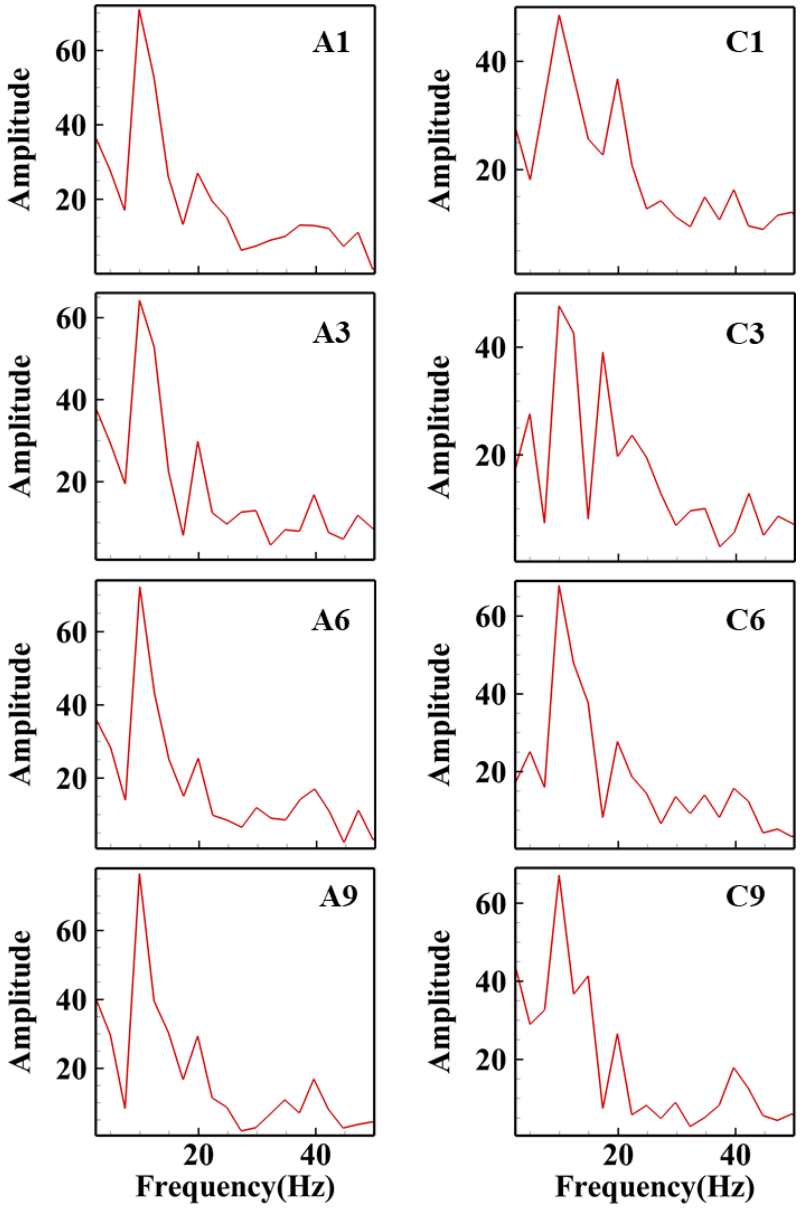

Fig. 10. The power spectrum of the pressure coefficients at the (a) wall of the draft tube (the right column) and (b) center of the draft tube (the left column). The signals are acquired at the probe location A1 and C1 (the first row), A3 and C3 (the second row), A6 and C6 (the third row), and A9 and C9 (the last row)

The frequency of fluctuations appears to be consistent across different probe locations, as detailed in Table 3. Low-frequency fluctuations are observed at all probes, with the frequency magnitude being nearly uniform across all locations. This consistency reflects the elevated intensity

of pressure and the alleviated frequency of fluctuation, a consequence of the intense vortical activity stimulated by the formation of structured vortex precessions.

Table 3
The frequency corresponding to the highest amplitude for the pressure coefficient spectrographs

Probe locations	Draft tube wall (A)	Draft tube center (C)
1	9.952	9.931
2	9.952	9.931
3	9.952	9.931
4	9.952	9.941
5	9.952	9.931
6	9.930	9.941
7	9.952	9.931
8	9.945	9.931
9	9.945	9.931

The final metric for characterizing the flow instabilities is depicted in Figure 11, which illustrates the power generation as a function of the pump-turbine revolution. The predicted power generation is approximately 29.1 kW, with the amplitude of fluctuations in the power signal constituting about 3% of the total generated power. The presence of the vortex rope in the center of the draft tube is identified as the primary contributor to these higher amplitude fluctuations in the power generation signal, underscoring its significant impact on the operational stability of the pump-turbine system.

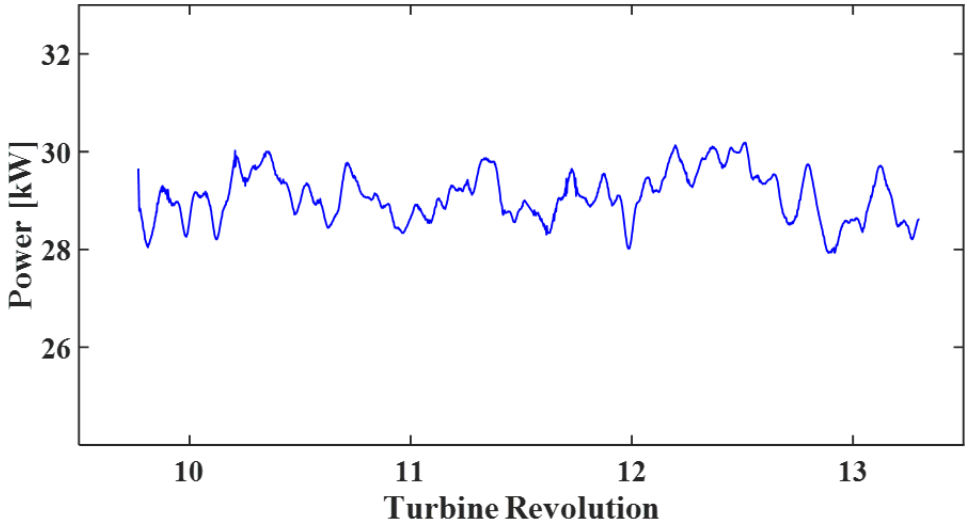

Fig. 11. The power signature as a function of the runner revolution

5. Conclusions

In a comprehensive large-eddy simulation of a pump-turbine system operating under 80% partial load, intricate flow and pressure fields were meticulously analyzed. The study characterized turbulent structures within the blade and draft tube regions, revealing a dominant, straight vortex rope extending from the blade exit to the draft tube outlet. This vortex rope, central to the draft tube, maintained its structure, creating centric stagnant area and influencing surrounding flow patterns. Pressure fluctuations reached up to 5% of the turbine head, with a noticeable pressure

surge associated with the vortex rope formation. Analysis using the Fast Fourier Transform of the pressure coefficient indicated a spectrum of both high-frequency, low-amplitude, and low-frequency, high-amplitude fluctuations, presenting potential risks to the structural integrity and operational stability of power generation. A discernible shear layer was noted between the swirling and central regions, highlighted by the differential fluid pressure and velocity along the radial direction of the draft tube. The turbine was reported to generate an average power of 29.1 kW, with the power signal exhibiting minor fluctuations attributed to vortical activities near the runner region, the vortex rope, and the corresponding pressure fluctuations.

Acknowledgement
This work used the Extreme Science and Engineering Discovery Environment (XSEDE) supported by National Science Foundation grant number TG-CTS170051. Specifically, the Bridges system at the Pittsburgh Supercomputing Center (PSC) is used for simulations.

References

[1] Lai, Xi-De, Quan-Wei Liang, Dao-Xing Ye, Xiao-Ming Chen, and Mi-Mi Xia. "Experimental investigation of flows inside draft tube of a high-head pump-turbine." *Renewable energy* 133 (2019): 731-742. https://doi.org/10.1016/j.renene.2018.10.058

[2] Goyal, Rahul, Michel J. Cervantes, and Bhupendra K. Gandhi. "Vortex rope formation in a high head model Francis turbine." *Journal of Fluids Engineering* 139, no. 4 (2017): 041102. https://doi.org/10.1115/1.4035224

[3] Nikolaos, Papadakis C., Fafalakis Marios, and Katsaprakakis Dimitris. "A review of pumped hydro storage systems." *Energies* 16, no. 11 (2023): 4516. https://doi.org/10.3390/en16114516

[4] Joy, Jesline, Mehrdad Raisee, and Michel J. Cervantes. "Experimental investigation of an adjustable guide vane system in a Francis turbine draft tube at part load operation." *Renewable Energy* 210 (2023): 737-750. https://doi.org/10.1016/j.renene.2023.04.096

[5] Liu, Gongcheng, Xudi Qiu, Jiayi Ma, Diyi Chen, and Xiao Liang. "Influence of flexible generation mode on the stability of hydropower generation system: Stability assessment of part-load operation." *Energies* 15, no. 11 (2022): 3956. https://doi.org/10.3390/en15113956

[6] Li, Huanhuan, Diyi Chen, Hao Zhang, Feifei Wang, and Duoduo Ba. "Nonlinear modeling and dynamic analysis of a hydro-turbine governing system in the process of sudden load increase transient." *Mechanical Systems and Signal Processing* 80 (2016): 414-428. https://doi.org/10.1016/j.ymssp.2016.04.006

[7] Trivedi, Chirag, Einar Agnalt, and Ole Gunnar Dahlhaug. "Experimental study of a Francis turbine under variable-speed and discharge conditions." *Renewable Energy* 119 (2018): 447-458. https://doi.org/10.1016/j.renene.2017.12.040

[8] Fortov, V. E., M. P. Fedorov, and V. V. Elistratov. "Scientific and technological problems of the hydropower industry after the accident at the Sayano-Shushenskaya hydropower plant." *Herald of the Russian Academy of Sciences* 81, no. 4 (2011): 333-340. https://doi.org/10.1134/S1019331611040010

[9] Subramanya, K., and Thanga Raj Chelliah. "Capability of synchronous and asynchronous hydropower generating systems: A comprehensive study." *Renewable and Sustainable Energy Reviews* 188 (2023): 113863. https://doi.org/10.1016/j.rser.2023.113863

[10] Roig, Rafel, Xavier Sánchez-Botello, Oscar de la Torre, Xavier Ayneto, Carl-Maikel Högström, Berhanu Mulu, and Xavier Escaler. "Fatigue damage analysis of a Kaplan turbine model operating at off-design and transient conditions." *Structural Health Monitoring* 23, no. 3 (2024): 1687-1700. https://doi.org/10.1177/14759217231191417

[11] Manogaran, Thiennieesh, Mohd Remy Rozainy Mohd Arif Zainol, Muhammad Khairi A. Wahab, Mohd Sharizal Abdul Aziz, Nurhanani Abd Aziz, Nazirul Mubin Zahari, Mohd Hafiz Zawawi, and Mohd Rashid Mohd Radzi. "Free-Surface Vortices Mitigation using Anti-Vortex Plates in Dam Intakes through CFD." *CFD Letters* 15, no. 6 (2023): 26-41. https://doi.org/10.37934/cfdl.15.6.2641

[12] Iovănel, Raluca G., Georgiana Dunca, Diana M. Bucur, and Michel J. Cervantes. "Numerical simulation of the flow in a Kaplan turbine model during transient operation from the best efficiency point to part load." *Energies* 13, no. 12 (2020): 3129. https://doi.org/10.3390/en13123129

[13] Masoodi, Faiz Azhar, and Rahul Goyal. "Aspects of vortex breakdown phenomenon in hydraulic turbines." *Experimental Thermal and Fluid Science* 150 (2024): 111051. https://doi.org/10.1016/j.expthermflusci.2023.111051

[14] Lihui, Xu, Guo Tao, and Wang Wenquan. "Effects of vortex structure on hydraulic loss in a low head Francis turbine under overall operating conditions base on entropy production method." *Renewable Energy* 198 (2022): 367-379. https://doi.org/10.1016/j.renene.2022.08.084
[15] Trivedi, Chirag. "A systematic validation of a Francis turbine under design and off-design loads." *Journal of Verification, Validation and Uncertainty Quantification* 4, no. 1 (2019): 011003.https://doi.org/10.1115/1.4043965
[16] Wu, Yulin, Jintao Liu, Yuekun Sun, Shuhong Liu, and Zhigang Zuo. "Numerical analysis of flow in a Francis turbine on an equal critical cavitation coefficient line." *Journal of Mechanical Science and Technology* 27 (2013): 1635-1641. https://doi.org/10.1007/s12206-013-0410-6
[17] Goyal, Rahul, Michel J. Cervantes, Faiz Azhar Masoodi, and Pallav Sahu. "A study of the velocity field during mitigation of vortex breakdown in model francis turbine at high load." *Journal of Fluids Engineering* 145, no. 4 (2023): 041203. https://doi.org/10.1115/1.4056614
[18] Trivedi, Chirag, Michel J. Cervantes, Bhupendra K. Gandhi, and Ole G. Dahlhaug. "Experimental and numerical studies for a high head Francis turbine at several operating points." *Journal of Fluids Engineering* 135, no. 11 (2013): 111102. https://doi.org/10.1115/1.4024805
[19] Nicolet, Christophe. *Hydroacoustic modelling and numerical simulation of unsteady operation of hydroelectric systems*. No. 3751. Epfl, 2007. https://doi.org/10.1109/PCT.2007.4538459
[20] Antonsen, Øyvind. "Unsteady flow in wicket gate and runner with focus on static and dynamic load on runner." (2007).
[21] Lai, Xide, Xiaoming Chen, Quanwei Liang, Daoxing Ye, Qiuqin Gou, Rongtao Wang, and Yi Yan. "Experimental and numerical investigation of vortex flows and pressure fluctuations in a high-head pump-turbine." *Renewable Energy* 211 (2023): 236-247. https://doi.org/10.1016/j.renene.2023.04.092
[22] Yu, An, Zhipeng Zou, Daqing Zhou, Yuan Zheng, and Xianwu Luo. "Investigation of the correlation mechanism between cavitation rope behavior and pressure fluctuations in a hydraulic turbine." *Renewable Energy* 147 (2020): 1199-1208. https://doi.org/10.1016/j.renene.2019.09.096
[23] Nicolet, Christophe, Amirreza Zobeiri, Pierre Maruzewski, and François Avellan. "On the upper part load vortex rope in Francis turbine: Experimental investigation." In *IOP Conference Series: Earth and Environmental Science*, vol. 12, no. 1, p. 012053. IOP Publishing, 2010. https://doi.org/10.1088/1755-1315/12/1/012053
[24] Altimemy, Muhannad, Bashar Attiya, Cosan Daskiran, I-Han Liu, and Alparslan Oztekin. "Mitigation of flow-induced pressure fluctuations in a Francis turbine operating at the design and partial load regimes—LES simulations." *International Journal of Heat and Fluid Flow* 79 (2019): 108444. https://doi.org/10.1016/j.ijheatfluidflow.2019.108444
[25] Jin, Faye, Puxi Li, Ran Tao, Ruofu Xiao, and Di Zhu. "Study of vortex rope for the flow field pulsation law." *Ocean Engineering* 273 (2023): 114026. https://doi.org/10.1016/j.oceaneng.2023.114026
[26] Foroutan, Hosein, and Savas Yavuzkurt. "A partially-averaged Navier–Stokes model for the simulation of turbulent swirling flow with vortex breakdown." *International Journal of Heat and Fluid Flow* 50 (2014): 402-416. https://doi.org/10.1016/j.ijheatfluidflow.2014.10.005
[27] Minakov, A. V., D. V. Platonov, A. A. Dekterev, A. V. Sentyabov, and A. V. Zakharov. "The numerical simulation of low frequency pressure pulsations in the high-head Francis turbine." *Computers & Fluids* 111 (2015): 197-205. https://doi.org/10.1016/j.compfluid.2015.01.007
[28] Skripkin, Sergey, Mikhail Tsoy, Pavel Kuibin, and Sergey Shtork. "Swirling flow in a hydraulic turbine discharge cone at different speeds and discharge conditions." *Experimental Thermal and Fluid Science* 100 (2019): 349-359. https://doi.org/10.1016/j.expthermflusci.2018.09.015
[29] Litvinov, Ivan, Sergey Shtork, Evgeny Gorelikov, Andrey Mitryakov, and Kemal Hanjalic. "Unsteady regimes and pressure pulsations in draft tube of a model hydro turbine in a range of off-design conditions." *Experimental Thermal and Fluid Science* 91 (2018): 410-422. https://doi.org/10.1016/j.expthermflusci.2017.10.030
[30] Nicolet, Christophe, Amirreza Zobeiri, Pierre Maruzewski, and François Avellan. "Experimental investigations on upper part load vortex rope pressure fluctuations in francis turbine draft tube." *International Journal of Fluid Machinery and Systems* 4, no. 1 (2011): 179-190. https://doi.org/10.5293/IJFMS.2011.4.1.179
[31] Muntean, S., C. Tănasă, A. I. Bosioc, and D. C. Moş. "Investigation of the plunging pressure pulsation in a swirling flow with precessing vortex rope in a straight diffuser." In *IOP Conference Series: Earth and Environmental Science*, vol. 49, no. 8, p. 082010. IOP Publishing, 2016. https://doi.org/10.1088/1755-1315/49/8/082010
[32] Trivedi, Chirag, Einar Agnalt, and Ole Gunnar Dahlhaug. "Investigations of unsteady pressure loading in a Francis turbine during variable-speed operation." *Renewable energy* 113 (2017): 397-410. https://doi.org/10.1016/j.renene.2017.06.005
[33] Jamali, Reza, Ali Sohani, Khosro Hemmatpour, Mohammadali Behrang, and Amin Ghobeity. "Experimental study of pressure pulsation in a large-scale hydropower plant with Francis turbine units and a common penstock." *Energy Conversion and Management: X* 16 (2022): 100308. https://doi.org/10.1016/j.ecmx.2022.100308

[34] Wu, H., F. Jin, Y. Luo, Y. Ge, Q. Wei, C. Zeng, X. Liu, W. Zhang, D. Miao, and H. Bai. "Suppressing the vortex rope oscillation and pressure fluctuations by the air admission in propeller hydro-turbine draft tube." *Journal of Applied Fluid Mechanics* 17, no. 1 (2023): 219-232. https://doi.org/10.47176/jafm.17.1.1994

[35] Sotoudeh, Nahale, Reza Maddahian, and Michel J. Cervantes. "Investigation of rotating vortex rope formation during load variation in a Francis turbine draft tube." *Renewable energy* 151 (2020): 238-254. https://doi.org/10.1016/j.renene.2019.11.014

[36] Amiri, Kaveh, Berhanu Mulu, Cervantes MJ, and Mehrdad Raisee. "Effects of load variation on a Kaplan turbine runner." International Journal of Fluid Machinery and Systems 9, no. 2 (2016): 182-193. https://doi.org/10.5293/IJFMS.2016.9.2.182

[37] Amiri, Kaveh, Berhanu Mulu, Mehrdad Raisee, and Michel J. Cervantes. "Unsteady pressure measurements on the runner of a Kaplan turbine during load acceptance and load rejection." *Journal of Hydraulic Research* 54, no. 1 (2016): 56-73. https://doi:10.1080/00221686.2015.1110626

[38] Amiri, Kaveh, Berhanu Mulu, Mehrdad Raisee, and M. J. Cervantes. "Load variation effects on the pressure fluctuations exerted on a Kaplan turbine runner." In *IOP Conference Series: Earth and Environmental Science*, vol. 22, no. 3, p. 032005. IOP Publishing, 2014. https://doi.org/10.1088/1755-1315/22/3/032005

[39] Valero, Carme, Mònica Egusquiza, David Valentín, Alexandre Presas, and Eduard Egusquiza. "Behavior of Francis turbines at part load. Field assessment in prototype: Effects on the hydraulic system." In *IOP Conference Series: Earth and Environmental Science*, vol. 240, no. 5, p. 052029. IOP Publishing, 2019. https://doi.org/10.1088/1755-1315/240/5/052029

[40] Müller, Andres, Arthur Favrel, Christian Landry, and François Avellan. "Fluid–structure interaction mechanisms leading to dangerous power swings in Francis turbines at full load." *Journal of Fluids and Structures* 69 (2017): 56-71. https://doi.org/10.1016/j.jfluidstructs.2016.11.018

[41] Valentín, David, Alexandre Presas, Eduard Egusquiza, Carme Valero, Mònica Egusquiza, and Matias Bossio. "Power swing generated in Francis turbines by part load and overload instabilities." *Energies* 10, no. 12 (2017): 2124. https://doi.org/10.3390/en10122124

[42] Sun, Longgang, Yanyan Li, Pengcheng Guo, and Zhuofei Xu. "Numerical investigation of air admission influence on the precessing vortex rope in a Francis turbine." *Engineering Applications of Computational Fluid Mechanics* 17, no. 1 (2023): 2164619. https://doi.org/10.1080/19942060.2022.2164619

[43] Zuo, ZhiGang, ShuHong Liu, DeMin Liu, and DaQing Qin. "Numerical predictions and stability analysis of cavitating draft tube vortices at high head in a model Francis turbine." *Science China Technological Sciences* 57 (2014): 2106-2114. https://doi.org/10.1007/s11431-014-5618-x

[44] Goyal, Rahul, Michel J. Cervantes, and Bhupendra K. Gandhi. "Characteristics of Synchronous and Asynchronous modes of fluctuations in Francis turbine draft tube during load variation." *International Journal of Fluid Machinery and Systems* 10, no. 2 (2017): 164-175. https://doi.org/10.5293/IJFMS.2017.10.2.164

[45] Nasir, Abdulbasit, Edessa Dribssa, and Misrak Girma. "The pump as a turbine: A review on performance prediction, performance improvement, and economic analysis." *Heliyon* (2024). https://doi.org/10.1016/j.heliyon.2024.e26084

[46] I. ANSYS, ANSYS Fluent users guide release 15.0, Canonsburg, PA, 2013.

[47] Nieuwstadt, F. T., Jerry Westerweel, and B. Boersma. *Introduction to theory and applications of turbulent flows*. Cham, Switzerland: Springer, 2016. https://doi.org/10.1007/978-3-319-31599-7

[48] Nicoud, Franck, and Frédéric Ducros. "Subgrid-scale stress modelling based on the square of the velocity gradient tensor." *Flow, turbulence and Combustion* 62, no. 3 (1999): 183-200. https://doi.org/10.1023/A:1009995426001

[49] Schleicher, W. C., and A. Oztekin. "Hydraulic design and optimization of a modular pump-turbine runner." *Energy conversion and management* 93 (2015): 388-398. https://doi.org/10.1016/j.enconman.2015.01.037

[50] Alfeuz, Abel, Fadzlita Tamiri, Farm Yan Yan, Wan Khairul Muzammil, Melvin Gan Jet Hong, Dayang Salyani Abang Mahmod, Nuramalina Bohari, and Mohd Azlan Ismail. "Performance Analysis of a Crossflow Vortex Turbine for a Gravitational Water Vortex Power Plant." *Journal of Advanced Research in Fluid Mechanics and Thermal Sciences* 116, no. 2 (2024): 13-26. https://doi.org/10.37934/arfmts.116.2.1326

[51] Penagos-Vasquez, Diego, Jonathan Graciano-Uribe, Luis Grisales-Noreña, Sebastián Vélez García, and Edward Andrés Torres-López. "Influence of Leading and Trailing Edge Angle on Impeller Blades of a Pump as Turbine." *Journal of Advanced Research in Fluid Mechanics and Thermal Sciences* 105, no. 1 (2023): 166-183. https://doi.org/10.37934/arfmts.105.1.166183

[52] Handoko, Rieky, Muhamad Dwi Septiyanto, Dominicus Danardono Dwi Prija Tjahjana, Dwi Aries Himawanto, Indri Yaningsih, and Syamsul Hadi. "Performance Testing and Analysis of Gravitational Water Vortex Turbine: A Modified Experimental Study on Blade Arc and Inclination Angle." *Journal of Advanced Research in Fluid Mechanics and Thermal Sciences* 109, no. 1 (2023): 147-161. https://doi.org/10.37934/arfmts.109.1.147161

[53] Prakoso, Aji Putro, Ahmad Fudholi, Deny Bayu Saefudin, Chairul Umam Rosyadi, Aris Suryadi, Ghalya Fikra, Yadi

Radiansyah, and Yusuf Suryo Utomo. "Effect of Cross-Sectional Depth on Horizontal and 30° Slop Spillway Open Channel Pico Hydro Cross-Flow Turbine Efficiency." *Journal of Advanced Research in Fluid Mechanics and Thermal Sciences* 113, no. 1 (2024): 176-187. https://doi.org/10.37934/arfmts.113.1.176187

[54] Setiawan, Dibyo. "Experimental and Numerical Study on Conical Gravitational Water Vortex Turbine with 3D Runner." *Journal of Advanced Research in Fluid Mechanics and Thermal Sciences* 114, no. 2 (2024): 1-14. https://doi.org/10.37934/arfmts.114.2.114

[55] Ramdhani, Muhammad Rasyid, Ridho Irwansyah, and Dendy Adanta. "Investigation of the 16 blades Pico Scale Breastshot Waterwheel performance in actual river condition." *Journal of Advanced Research in Fluid Mechanics and Thermal Sciences* 75, no. 1 (2020): 38-47. https://doi.org/10.37934/arfmts.75.1.3847

[56] Turbines, Hydraulic. "Storage Pumps and Pump-Turbines—Model Acceptance Tests; IEC Standard 60193." *International Electrotechnical Commission (IEC): Geneva, Switzerland* (1999).

[57] Ji, B., X. W. Luo, Roger EA Arndt, Xiaoxing Peng, and Yulin Wu. "Large eddy simulation and theoretical investigations of the transient cavitating vortical flow structure around a NACA66 hydrofoil." *International Journal of Multiphase Flow* 68 (2015): 121-134. https://doi.org/10.1016/j.ijmultiphaseflow.2014.10.008

[58] Chen, Ying, Xin Chen, Jie Li, Zhaoxin Gong, and Chuanjing Lu. "Large eddy simulation and investigation on the flow structure of the cascading cavitation shedding regime around 3D twisted hydrofoil." *Ocean Engineering* 129 (2017): 1-19. https://doi.org/10.1016/j.oceaneng.2016.11.012

[59] Dörfler, Peter, Mirjam Sick, and André Coutu. *Flow-induced pulsation and vibration in hydroelectric machinery: engineer's guidebook for planning, design and troubleshooting*. London: Springer, 2013. https://doi.org/10.1007/978-1-4471-4252-2